Effect of Yb^{3+} doping level on the structure and spectroscopic properties of ZnO optical ceramics

Effect of Yb^{3+} doping level on the structure and spectroscopic properties of ZnO optical ceramics

E Gorokhova[1], I Venevtsev[2], I Alekseeva[1], A Khubetsov[1], O Dymshits[1], L Basyrova[3], E Oreschenko[1], S Eron'ko[1], F Muktepavela[4], K. Kundzins[4], A Zhilin[1] and P Loiko[3]

[1] S.I. Vavilov State Optical Institute, 36 Babushkina St., 192171 St. Petersburg, Russia
[2] Peter the Great St. Petersburg Polytechnic University, 29 Polytechnic St., 195251 St. Petersburg, Russia
[3] Centre de Recherche sur les Ions, les Matériaux et la Photonique (CIMAP), UMR 6252 CEA-CNRS-ENSICAEN, Université de Caen Normandie, 6 Boulevard du Maréchal Juin, 14050 Caen Cedex 4, France
[4] Institute of Solid State Physics, University of Latvia, 8 Kengaraga St., LV1063, Riga, Latvia

e.gorokhova@rambler.ru; khubezov@gmail.com;

Abstract. Zinc oxide optical ceramics with hexagonal structure doped with 0.6 –5.0 wt% Yb were fabricated by uniaxial hot pressing of commercial oxide powders at 1180 °C in vacuum. The ceramics were characterized by X-ray diffraction, SEM, EDX, X-ray and optical spectroscopy. It is shown that Yb^{3+} ions are distributed between C-type Yb_2O_3 sesquioxide crystals and ZnO grain boundaries. The Yb^{3+} doping of ZnO ceramics enhances the near-band-edge emission of zinc oxide. ZnO:Yb optical ceramics are promising for optoelectronic applications.

1. Introduction

Zinc oxide (ZnO) is a direct wide band gap semiconductor with unique optical and luminescent properties coupled with high radiation tolerance. Ytterbium (Yb^{3+}) doped ZnO nanostructures and films demonstrate efficient energy transfer between the defect states in the ZnO structure and the dopant Yb^{3+} ions [1], making them promising for down-conversion layers of enhanced solar cells [2]. It has been shown that the efficient energy transfer from ZnO to Yb^{3+} ions in the nanocomposites is due to the formation of a tight contact between the Yb_2O_3 and ZnO nanoparticles (i.e., the Yb_2O_3-ZnO heterojunction) and it arises mainly from the quantum cutting mechanism [1]. In the present work, the effect of Yb doping level on the structure, optical and spectral-luminescent properties of hexagonal ZnO ceramics was studied for the first time.

2. Experimental

ZnO optical ceramics with an Yb doping level of 0.6– 5.0 wt% were fabricated from commercial reagent grade ZnO and Yb_2O_3 powders by hot pressing in vacuum at the temperature of 1180 °C. After polishing, ceramic disks had a diameter of 25 mm and a thickness of about 0.5 mm. The undoped ZnO

ceramic was pale yellow colored. With Yb^{3+} doping, the color of ceramics changed to slight grey and their transparency decreased, Figure 1.

The X-ray powder diffraction (XRD) patterns of ceramics were measured with a Shimadzu XRD-6000 diffractometer with Ni-filtered Cu Kα radiation. The ZnO unit cell parameters were determined by the Rietveld method. The texture coefficients were calculated from the XRD data using the approach described in Ref. [3]. The microstructure of the polished and etched surfaces of ceramics was characterized by scanning electron microscopy (SEM) using a MERLIN microscope (Carl Zeiss). The same microscope equipped with an Inca Energy X-Max analyzer was employed for the EDX-based element mapping. The fractured surfaces of ceramic disks were studied using a scanning electron microscope (SEM, TESCAN Lyra 3) equipped with an energy dispersive X-ray spectrometer EDS (Oxford, AZtec) in back scattering electron (BSE) mode.

The total transmittance spectra in the visible and near-IR were measured using a SPECORD 200 PLUS spectrophotometer. The absorption spectra at 300 – 3300 nm were measured with a Shimadzu UV-3600 spectrophotometer. The X-ray induced luminescence (XRIL) spectra were recorded in the reflection geometry upon continuous excitation by an X-ray tube with a tungsten anode (40 kV, 10 mA). The decay kinetics of XRIL was recorded using a pulsed X-ray setup with a pulse duration of ~1 ns at a voltage of 30 kV and a current amplitude of 500 mA.

Figure 1. Photographs of undoped and Yb^{3+}-doped ZnO transparent ceramics with increasing Yb doping level (from left to right). The labels indicate the Yb concentration (in wt%).

3. Results and discussion

A typical XRD pattern of Yb^{3+}-doped ZnO ceramic is shown in Figure 2(a). The XRD patterns of the Yb:ZnO ceramics evidence crystallization of hexagonal (sp. gr. $P6_3mc$) phase of ZnO with wurtzite structure and Yb_2O_3 with a cubic (sp. gr. $Ia\bar{3}$) C-type bixbyite structure. The calculated ZnO unit cell parameters for the Yb^{3+}-doped ceramics nearly coincide with those for undoped ZnO (a = 3.249 Å, c = 5.205 Å, International Centre for Diffraction Data (ISDD) card No. 5-0664). They do not change with increasing the Yb content indicating that Yb^{3+} ions do not enter the ZnO structure. The fragment of the XRD pattern in the range of diffraction angles 2θ of 29.0 - 30.3° contains an unambiguously assigned intense diffraction peak of Yb_2O_3 with the Miller's index (hkl) = (222), Figure 2(b). The volume fraction of Yb_2O_3 in ceramics gradually increases with Yb content, Figure 2(c). The EDX mapping indicates that Yb^{3+} ions are also localized at the ZnO grain boundaries, Figure 2(d-f).

We performed the SEM study of fractured surfaces of Yb^{3+}-doped ZnO ceramics with the aim to determine the arrangement and location of Yb_2O_3 crystals. The corresponding SEM images for the ZnO: 0.6wt% Yb and ZnO: 3wt% Yb ceramics, cf. Figure 3(a,b), indicate the intragranular fracture mechanism. We failed to find any evidence of brittle fracture on the grain boundaries. This testifies a sufficient strength of ceramics that ensures their reliability in use. The comparison of images presented in Figure 3(a,b) demonstrates that with increasing the ytterbium doping level, the volume fraction of Yb_2O_3 crystals significantly increases.

The Yb_2O_3 crystals are formed in different places within the ZnO ceramic, namely (i) at the grain boundaries (GB) with highest probability, Figure 3(c), (ii) in triple joints of the ZnO grains, which will be shown below, and between the ZnO planes, Figure 3(d). The Yb_2O_3 crystals form regions with sizes ranging from 2-5 to 15-20 μm. These regions are built from smaller grains with sizes of 0.2 -1.0 μm. Their destruction occurs by the quasi-brittle cleavage. The Yb_2O_3 crystals located at the GBs of ZnO grains have sufficient adhesion to ZnO, which indicates strong interaction at the GBs of these oxides. This is evidenced by the SEM-EDX studies of the ZnO:Yb ceramics with different locations of Yb_2O_3

crystals (at the GBs and inside the grains). As an example, Figure 4 shows the SEM-EDX data for the ZnO:0.6wt% Yb ceramic, wherein the grain of Yb_2O_3 is located at the triple joint and partially inside the ZnO grain.

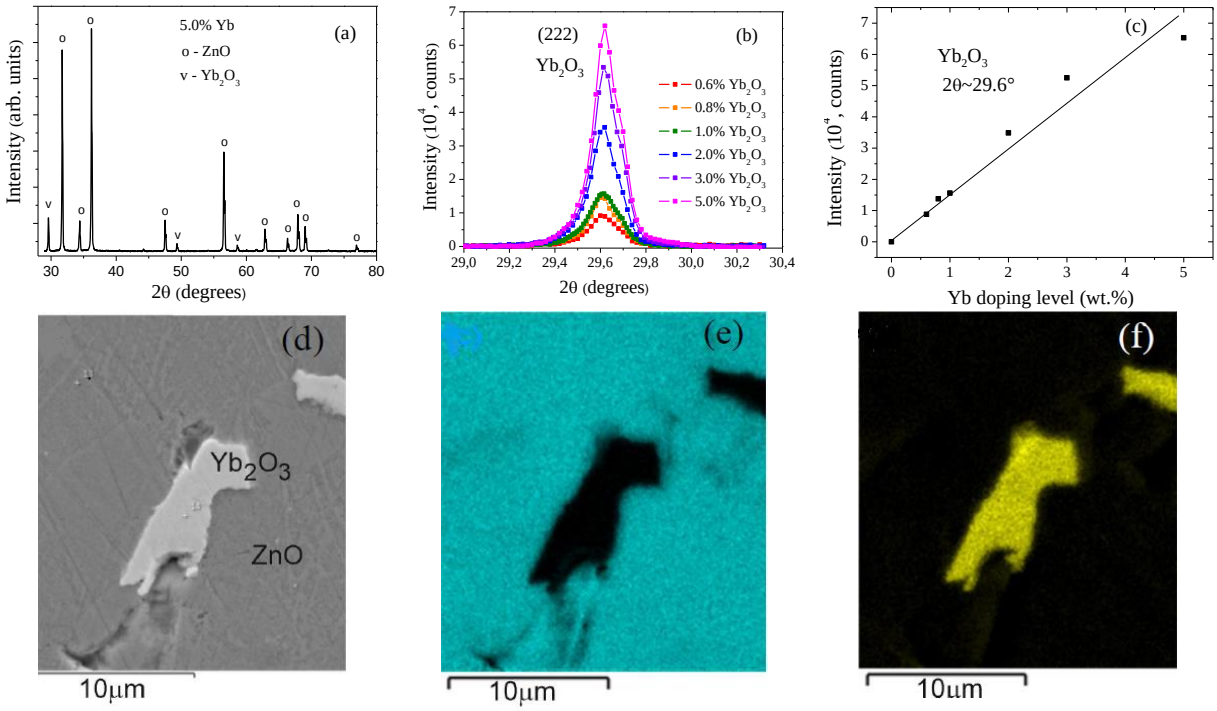

Figure 2. (a) XRD pattern of ZnO:5 wt% Yb ceramic; **(b)** XRD patterns of ZnO:Yb ceramics with different Yb doping level in the 2θ range of 29.0 - 30.3° corresponding to the (222) reflection of cubic Yb_2O_3; **(c)** the dependence of the XRD peak intensity at 2θ ~29.6° on the Yb^{3+} concentration; **(d)** SEM image of the polished and etched surface of the ZnO:2 wt% Yb ceramic; **(e,f)** EDX element mapping of **(e)** Zn (Lα) and **(f)** Yb (Mα).

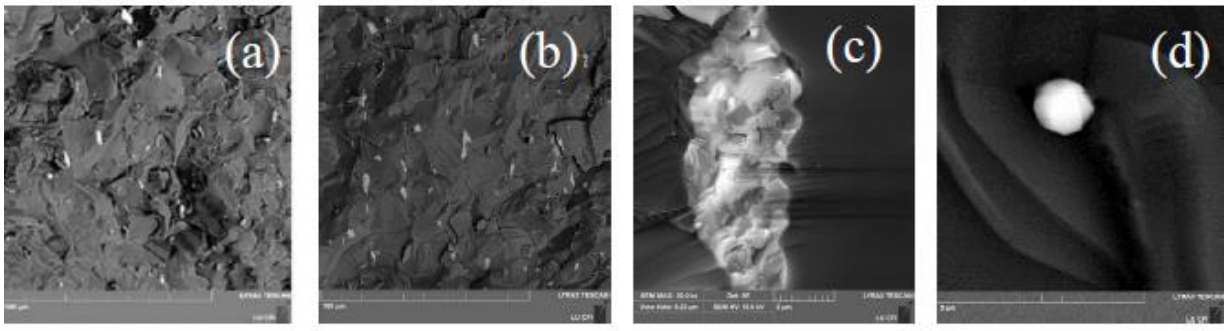

Figure 3. SEM images of the fractured surfaces of ZnO:0.6 wt% Yb **(a)** and ZnO:3 wt% Yb ceramics **(b)**; various localizations of Yb_2O_3 crystals in the ZnO ceramics **(c,d)**.

According to the EDX data for the ZnO:0.6 wt% Yb ceramic, 2.6 wt% Zn is found in the Yb_2O_3 crystal. It seems likely to appear from the surrounding ZnO ceramic body. There are no Yb ions within the ZnO grain. Perhaps this is due to the small ytterbium doping level in this sample, since for the ZnO:3.0 wt% Yb ceramic, 0.2 wt% Yb were detected within the ZnO grain. The EDX data prove the interaction at the GBs of the two oxide phases despite a significant difference in their unit cell parameters (for ZnO, a = 3.249 Å, c = 5.205 Å; for Yb_2O_3, a = 10.441 Å) and ionic radii (ionic radius of $^{IV}Zn^{2+}$ = 0.600 Å, while that of $^{VI}Yb^{3+}$ = 0.868 Å). Considering the high adhesion at the interfaces of

ZnO and Yb_2O_3 grains, we can assume the leading role of the special (nonequilibrium) state of the electronic structure of the GBs in the processes of interaction and transfer of excitation energy from ZnO to Yb^{3+} ions. The previous study by Qi *et al*. [4] of the properties of boundaries in nonequilibrium conditions confirms this possibility.

The analysis of the texture of the ZnO:Yb ceramics indicated that the main components of the texture are the (100) and (110) planes of the hexagonal prism and the (101) planes of the hexagonal pyramid, whose texture coefficient values are significantly higher than those of pure ZnO ceramic.

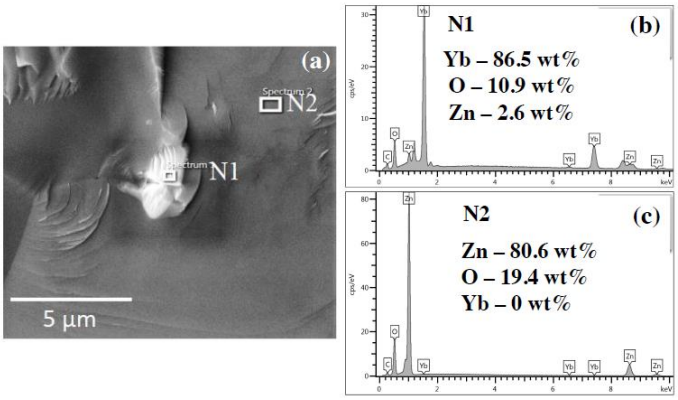

Figure 4. SEM image of a fractured surface of the ZnO:0.6wt% Yb ceramic with the indicated places of spectral analysis **(a)**; spectrum 1 from the Yb_2O_3 grain **(b)**, spectrum 2 from the ZnO grain **(c)**, insets in **(b,c)** - the weight percentages of Zn, O and Yb elements.

The average ZnO grain size of ZnO:Yb ceramics (10-15 µm) practically does not depend on the Yb concentration and is much smaller than that of the undoped ceramic. The inhibitory effect of Yb on the growth of ZnO grains is due to the fact that this impurity is not incorporated into the zinc oxide lattice but is adsorbed at the active surfaces of the crystals, as well as forms crystals of Yb_2O_3 preventing the excessive growth of ZnO crystals.

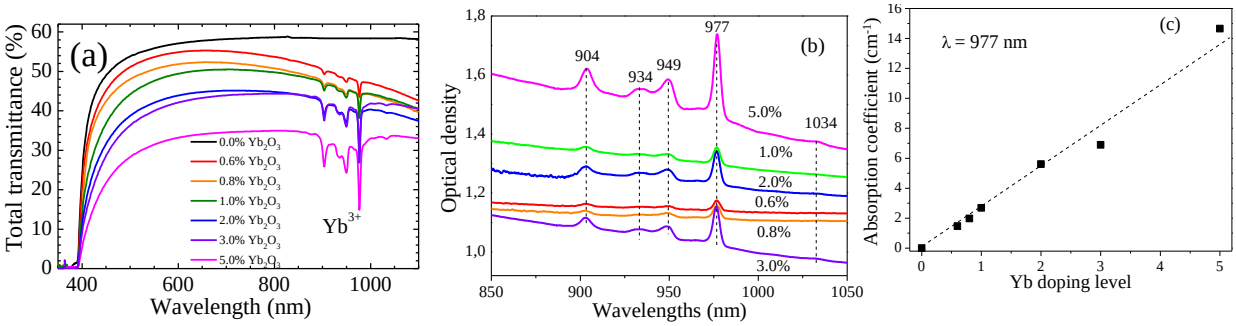

Figure 5 (a-c). Optical spectroscopy of ZnO:Yb optical ceramics: (**a**) total transmittance spectra, thickness: ~0.5 mm; absorption spectra in the range of 850 - 1050 nm (**b**), dependence of the decimal absorption coefficient at the wavelength of 977 nm on the Yb doping level (**c**).

The total transmittance spectra of ZnO and ZnO:Yb ceramics are shown in Figure 5(a). The spectra of Yb:ZnO ceramics contain the characteristic Yb^{3+} absorption band due to the $^2F_{7/2} \rightarrow {}^2F_{5/2}$ transition. The maximum value of total transmittance in the visible decreases from ~55% to 35% with increasing the Yb content from 0.6 to 5.0 wt%. The addition of Yb also results in shifts of the UV and IR absorption edges of ceramics in opposite directions. There is a shift by 10 nm, from 0.38 to 0.39 µm in the UV and from 4.0 to 2.5-2.7 µm, in the IR spectral range. The latter effect is assigned to increased concentration of free carriers in ZnO, from 3.1×10^{18} cm^{-3} to 7.4–8.0×10^{18} cm^{-3}, as calculated using the approach described in Ref. [5]. Figure 5(b) focuses on the Yb^{3+} absorption. The shape of the absorption band of Yb^{3+} ions does not depend on the doping concentration, which suggests that the site

symmetry for these ions does not change with their concentration. The almost linear dependence of the absorption coefficient on the concentration of Yb^{3+} ions at the wavelength of 977 nm indicates the implementation of the Beer's law, Figure 5(c).

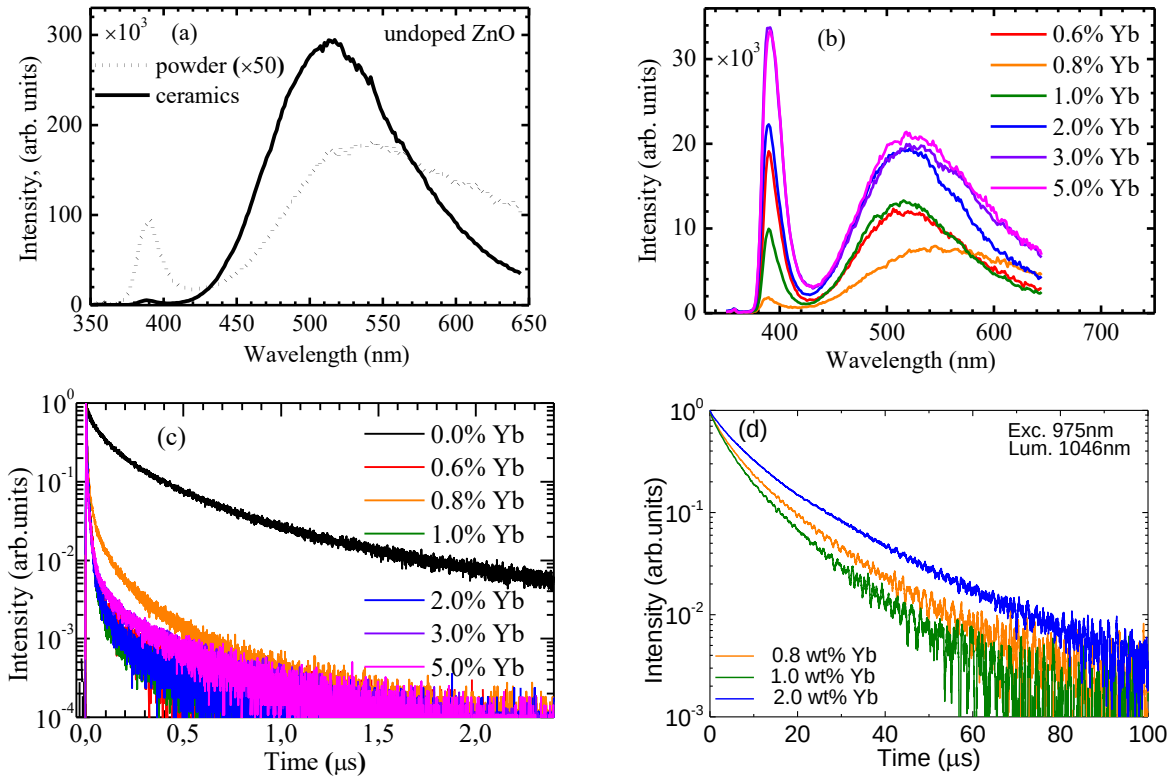

Figure 6(a-d). The spectra of X-ray luminescence of **(a)** the initial ZnO powder and undoped ZnO ceramics and **(b)** Yb^{3+}-doped ZnO ceramics; **(c)** X-ray luminescence decay curves; **(d)** luminescence decay curves for Yb^{3+} ions, $\lambda_{exc} = 975$ nm, $\lambda_{lum} = 1046$ nm.

The X-ray luminescence spectra of the initial ZnO powder, undoped ZnO and ZnO:Yb ceramics contain two emission bands, Figure 6(a,b). One of them is a narrow UV band located near the absorption edge, called the near-band-edge (NBE) emission of an excitonic nature. Another broad band located in the green region of the spectrum is the so-called deep level (DL) emission. The DL emission is usually associated with intrinsic point defects, the exact type of which is still a matter of debate. The DL luminescence is often ascribed to oxygen vacancies. The spectrum of the initial ZnO powder exhibits a weak NBE band with a maximum at 388 nm and a two-times more intense DL band centered at 530 nm. Intensity of the NBE band of the undoped ZnO ceramic is comparable to that of the initial powder. On the contrary, intensity of the DL band of undoped ceramic with a maximum at 513 nm is ~80 times higher than that of the powder. Most likely, this increase in intensity is due to an increase in the concentration of oxide vacancies under the conditions of high-temperature deformation during uniaxial hot pressing in vacuum. It has been widely reported that exposure to high pressure can cause a high concentration of vacancies in ZnO [5]. Intensity of the DL luminescence with a maximum at 520-521 nm for ZnO:Yb ceramics is by an order of magnitude weaker than that for the undoped ceramic. In contrast, intensity of the NBE emission bands of the ZnO:Yb ceramics is higher than that for the undoped ZnO. With increasing the Yb concentration, intensity of the NBE emission increases and saturates for 5 wt% Yb doping. The position of its maximum slightly shifts from 390 to 391 nm probably due to a change in the energy band structure. A similar effect of increasing intensity of the exciton luminescence and decreasing intensity of the DL emission associated with oxide defects upon the addition of Yb^{3+} ions to the ZnO nanopowders was observed by Kabongo *et al.* [6]. The

authors assigned these data either to a possible energy transfer from Yb^{3+} ions to ZnO or to a reduction of oxygen related defects.

The Yb doping accelerates the decay of ZnO luminescence, Figure 6(c), although no clear correlation between its content and the shape of the decay curves can be found. With increasing the Yb doping level, the shape of the XRIL kinetics of ZnO:Yb ceramics changes only slightly. The decay curves are not single exponential. For all the studied samples, they can be divided into two time domains: 0-50 ns and 200-2000 ns. The first range mainly contains a "fast" component with a decay time of 7-15 ns for all the studied Yb^{3+}-doped ceramics. For the undoped sample, the characteristic decay time in this region is longer, ~ 50 ns. The second range corresponds to a "slow" decay time of ~ 390-430 ns in all the samples. The undoped ceramic and ceramic doped with 0.8% Yb are distinguished from other ceramics by a much slower decay recorded in the range of 50-500 ns, which correlates with smaller intensities of NBE emissions in comparison with those of the DL, as shown in Figure 6(a,b). It should be noted that the DL emission in the sample with 0.8% Yb is also shifted to longer wavelengths compared to that in other samples. One can assume that the main change in decay kinetics occurs for small (<0.6%) Yb contents.

The luminescence lifetimes of Yb^{3+} ions (the $^2F_{5/2}$ state) are about 10 μs and they are weakly dependent on the Yb doping level, Figure 6(d).

4. Conclusions

ZnO:Yb optical ceramics were fabricated for the first time. Yb^{3+} ions do not enter the ZnO structure while they are located on the ZnO grain surface and form the Yb_2O_3 crystals at the grain boundaries. The optical properties of ZnO:Yb ceramics indicate the ZnO ↔ Yb^{3+} energy-transfer. The study of the fracture mechanisms, phase composition and spectral data allowed us to reveal the role of the nonequilibrium state of the electronic structure of grain boundaries on the excitation energy transfer from ZnO to Yb^{3+} ions, which resulted in an increase of the near-band-edge emission intensity. The developed ceramics are promising for optoelectronic applications.

Acknowledgment

This work was partly supported by the RFBR (Grant 19-03-00855).

References

[1] Shestakov M, Baranov A, Tikhomirov V, Zubavichus Y, Kuznetsov A, Veligzhanin A, Kharin A, Rösslhuber R, Timoshenko V and Moshchalkov V 2012 *RSC Adv.* **2** 8783
[2] Balestrieri M, Ferblantier G, Colis S, Schmerber G, Ulhaq-Bouillet C, Muller D, Slaoui A and Dinia A 2013 *Sol. Energy Mater. Sol. Cells* **117** 363
[3] Márquez J A R , Rodríguez C M B , Herrera C M, Rosas E R, Angel O Z and Pozos O T **2011** *J. Electrochem. Sci.* **6** 4059
[4] Qi Y, Kauffmann Y, Kosinova A, Kilmametov A R, Straumal B B and Rabkin E 2021 *Mater. Res. Lett.* **9** 58
[5] Yang X, Electrical and optical properties of zinc oxide for scintillator applications, 2008 *Graduate Theses, Dissertations, and Problem Reports* 2729 https://researchrepository.wvu.edu/etd/2729 106
[6] Kabongo G L, Mhlongo G H, Mothudi B M, Hillie K T, Swart H C and Dhlamini M S 2014 *Mater. Lett.* **119** 71